



## ABSTRACT

Oxygenated organic molecules (OOMs) are dominated by the N-containing species in polluted urban environment. As N-containing OOMs, especially those with more than one nitrogen atoms, prevailed in the high  $m/z$  range ( $m/z > 350$ Th), unambiguous identification of N-containing OOMs is highly desirable for understanding of their formation processes, precursors and influencing factors. To achieve this, we applied an ultra-high-resolution chemical ionization-orbitrap (CI-Orbitrap) in a field campaign and found that OOMs contain one (1N-OOMs), two (2N-OOMs) and three (3N-OOMs) nitrogen atoms respectively comprised 50%, 26% and 4% of total OOMs. More interestingly, the fraction of 2N-OOMs increased with the increase of carbon number ( $nC$ ) and were dominated by the ones derived from aliphatic precursors (2N-OOM<sub>Ali</sub>, 64.2%), indicating the importance of multistep oxidation. Plausible precursors of 2N-OOMs were aliphatics (2N-OOM<sub>Ali</sub>, 64.2%), aromatics (2N-OOM<sub>Aro</sub>, 16%), and monoterpenes (2N-OOM<sub>MT</sub>, 15.4%). The absolute concentrations of 2N-OOMs were greatly affected by the pollution level for the most cases. The 2N-OOM<sub>Ali</sub> was the most abundant 2N-OOMs and its fraction even increased in the polluted day with enhanced proportion of the ones with  $nC > 10$ . While 2N-OOM<sub>Ali</sub> and 2N-OOM<sub>Aro</sub> were dominated by daytime photochemical production, nighttime NO<sub>3</sub>-initiated oxidation played a comparable role as the daytime photochemistry in the formation of 2N-OOM<sub>MT</sub>. 2N-OOM<sub>Aro</sub> were of highest oxygenation level, followed by 2N-OOM<sub>MT</sub> and 2N-OOM<sub>Ali</sub>, which were affected by photochemistry and NO<sub>x</sub> concentrations. These results highlight the significant formation of 2N-OOMs and the influencing factors, on their formation in polluted urban environment, where various VOC precursors and atmospheric oxidants present.

## 37 **1. Introduction**

38 Secondary organic aerosol (SOA) accounts for a significant fraction of particulate matters (Donahue  
39 et al., 2009; Ehn et al., 2014; Hallquist et al., 2009; Jimenez et al., 2009). Volatile organic compounds  
40 (VOCs) and their oxidation products, *i.e.*, OVOCs, are important precursors of SOA in the atmosphere  
41 (Atkinson and Arey, 2003; Bianchi et al., 2019; Ehn et al., 2014; Nie et al., 2022). The N-containing  
42 oxygenated organic molecules (OOMs) have been identified as the important products upon VOC  
43 oxidation. Especially at high NO<sub>x</sub> levels, these products become more dominant while the others  
44 (*i.e.*, alcohols, hydroperoxides and RO<sub>2</sub> cross-reaction products) are likely suppressed (Bianchi et al., 2019;  
45 Zhao et al., 2018). The nitrogen atoms in OOM molecules are assumed to be mainly associated with nitrate  
46 group (-ONO<sub>2</sub>) formed from bi-molecular reaction between RO<sub>2</sub> radical and NO. Field measurements also  
47 observed that up to 77 % of molecules in organic aerosol (OA) contain nitrate functional groups under  
48 different atmospheric conditions (Ditto et al., 2020; Kenagy et al., 2021; Kiendler-Scharr et al., 2016; Lee  
49 et al., 2016; Lee Ng et al., 2017; Lin et al., 2021; Rollins et al., 2013; Xu et al., 2015; Ye et al., 2021; Yu  
50 et al., 2019).

51 The N-containing OOM molecules can be classified into 1N-OOMs, 2N-OOMs, and 3N-OOMs,  
52 according to the number of N atoms in the molecule. The chemical composition of N- containing OOMs  
53 is determined by their precursors, formation pathways and NO<sub>x</sub> level in the atmosphere (Bianchi et al.,  
54 2019; Ehn et al., 2014; Nie et al., 2022; Pye et al., 2019; Riva, 2016; Yan et al., 2016). Recent observations  
55 in megacities of China indicated that 2N-OOMs accounted for significant fractions (about 30-33%) among  
56 total N-containing OOMs besides 1N-OOMs (66-70%) due to the high NO<sub>x</sub> concentrations in polluted  
57 urban environment (Nie et al., 2022; Yan et al., 2021). Some laboratory studies also proposed that the  
58 potential formation pathways of 2N-OOMs, such as the multiple-step OH oxidation (Garmash et al., 2020)  
59 or the NO<sub>3</sub>-initiated oxidation followed by NO termination (Kiendler-Scharr et al., 2016; Liebmann et al.,  
60 2019), suggesting the increased importance of multi-step bimolecular oxidation in the formation of 2N-  
61 OOMs. On the other hand, it was also found that the formation of 2N-OOMs showed the clear preference  
62 of specific precursors compared to 1N-OOMs, *i.e.*, significantly higher branch ratio of 2N-OOMs from

63 aliphatic hydrocarbons than those from aromatics (Nie et al., 2022), suggesting considerable difference  
64 from 1N-OOMs in terms of formation pathway. Determining the formation pathway of N-containing  
65 OOM molecules, especially those containing two to three nitrogen atoms, in real atmosphere, is  
66 challenging. Identification of their chemical compositions in molecular level is the key for advancing our  
67 understanding in the precursor, formation and sources of N-containing OOMs in polluted atmosphere,  
68 where thousands of oxidation products exist and evolve constantly.

69 Traditionally, a chemical ionization atmospheric pressure interface time-of-flight mass spectrometer  
70 (CI-APi-TOF) has been used to measure the gaseous OOMs (Berndt et al., 2016; Ehn et al., 2014; Jokinen  
71 et al., 2014; Rissanen et al., 2014). Using a CI-APi-TOF, increasing number of studies have been reporting  
72 the formation of OOMs through the oxidation of various VOC precursors in chamber or flow tube (Berndt  
73 et al., 2016, 2018; Ehn et al., 2014; Garmash et al., 2020; Jokinen et al., 2014, 2015; Rissanen et al., 2014;  
74 Wang et al., 2020; Zhao et al., 2018). While 2N-OOMs in real ambient almost exclusively located in high  
75  $m/z$  (mass-to-charge) range (*i.e.*, 300 - 500 Th), a CI-APi-TOF with highest mass resolving power of  
76 12,000 ( $m/\Delta m$ , in full width at half maximum) at  $m/z=200$  Th and above, can hardly identify the molecular  
77 compositions of 2N-OOMs unambiguously. This is because low mass resolving power imposes significant  
78 uncertainties on separating overlapping peaks, which increases rapidly with increasing  $m/z$  and decreasing  
79 mass resolving power. Taken the integer  $m/z$  of 342 as an example, multiple peaks overlap at this nominal  
80 mass, *i.e.*,  $C_7H_8O_{10}N_2(NO_3)^-$  (342.0057 Th),  $C_8H_{12}O_9N_2(NO_3)^-$  (342.0421 Th),  $C_9H_{16}O_8N_2(NO_3)^-$   
81 (342.0785 Th),  $C_{10}H_{20}O_7N_2(NO_3)^-$  (342.1149 Th). The adjacent peaks are of mass differences ( $\Delta m$ ) of  
82 0.0364 and a good peak separation of these peaks ( $4\sigma$ ) requires mass resolving power of at least 16,000.  
83 Therefore, development and application of mass spectrometry techniques with extremely high  
84 performance in detection limit, time resolution, and mass resolving power, are highly desirable.

85 To achieve accurate identification of molecular formula from the extremely complex mass spectra, a  
86 CI (nitrate) inlet had also been coupled to an orbitrap mass spectrometer (CI-Orbitrap) to measure the  
87 OOMs in ultra-high mass resolving power ( $m/\Delta m > 100,000$  at  $m/z=200-500$  Th) (Riva et al., 2019a;  
88 Zhang et al., 2022). The ultra-high mass resolving power of CI-Orbitrap will undoubtedly provide

89 significant improvements in molecular identification, separation, and quantification. Herein, we applied a  
90 CI-Orbitrap in a field campaign for the measurements of OOMs, with a special focus on 2N-OOMs, in  
91 molecular level in urban Shanghai. The site represents a typical eastern Chinese megacity characterized  
92 by intense human activities, multiple anthropogenic emissions and high NO<sub>x</sub> concentrations. Based on the  
93 measurement results as well as our current knowledge on N-containing OOM formation, we classify the  
94 observed 2N-OOMs into different precursor groups and explore the potential influencing factors on their  
95 formation. Furthermore, supported by positive matrix factorization (PMF), sources and gas-phase  
96 oxidation processes for 2N-OOM formation in urban Shanghai were identified.

## 97 **2. Ambient measurement and methodology**

### 98 **2.1 Measurements**

99 The field campaign was carried out from 31<sup>th</sup> October to 18<sup>th</sup> November, 2020 on the top-floor of an  
100 8-story building in Shanghai Academy of Environmental Sciences (31° 18' N, 121° 43' E, [Figure S1](#)), which  
101 sits in a densely populated region surrounded by commercial properties and residential dwellings without  
102 significant industrial sources nearby. The site can represent a typical urban area of Shanghai affected by  
103 severe local emissions from vehicular traffic, commercial, and residential activities. Our campaign was  
104 carried out in autumn which represents a typical transition period from strong photochemistry in summer  
105 to intense regional transport in winter. At times, air masses transported from the neighboring provinces or  
106 even further from the northern China can also affect the air quality of the site.

107 The 2N-OOMs as well other OOMs molecules were measured in real time with a nitrate-Orbitrap.  
108 The operation of nitrate-Orbitrap has been detailed in previous studies as well as in one of our companion  
109 studies (Zhang et al., 2022), thus is only briefly described here. Ambient air was drawn into the ionization  
110 source through a 1m stainless-steel tube (3/4 inch). The reagent ion was produced by passing nitric acid  
111 in sheath flow (20L/min) into a PhotoIonizer (Model L9491, Hamamatsu, Japan) and was then introduced  
112 into a co-axial laminar flow reactor, in which the reagent ions interact with the air samples. The charged  
113 species were detected by an orbitrap mass analyzer with a [mass resolving power](#) of about 140,000. Mass-  
114 dependent transmission calibrations was also performed using a depletion method (Heinritzi et al., 2016).

115 Other ancillary measurements, including the PM<sub>2.5</sub> concentrations, trace gases (SO<sub>2</sub>, O<sub>3</sub> and NO<sub>x</sub>), volatile  
116 organic compounds, as well as meteorological parameters (wind direction and speed, solar radiation, etc.)  
117 were detailed in Supporting Information (SI-1). An overview of the measurement data, illustrating the air  
118 quality as well as the meteorological conditions during the campaign, is provided in SI-2 and Figure S2.

## 119 2.2 Data analysis of nitrate CI-Orbitrap

120 The raw mass spectra were first extracted by Orbitool (Cai et al., 2020) and the molecular information  
121 was then achieved by applying a homemade toolkit based on the MATLAB software. The toolkit drew on  
122 the idea from “tofTools” package which is used for analyzing the mass spectral data obtained from the  
123 TOF analyzer, such as nitrate CI-API-TOF (Junninen et al., 2010). The concentrations of the detected  
124 species are then determined as follows:

$$125 [X] = \frac{i[X^-]}{NO_3^- \cdot (HNO_3)_{0-2}} \cdot C \quad (1)$$

126 where  $i[X^-]$  is the transmission-corrected signal intensity of ion X in unit of counts per second (cps),  $C$   
127 represents the calibration factor.  $C$  is determined from the collision frequency of target species with the  
128 nitrate ions (cluster) during its residence in the charger, taking into account of the losses onto the walls of  
129 the reactor and the tube (Eq. 2):

$$130 C = C_{H_2SO_4} = \frac{1}{k_{ion} \times RT \times f_{inlet}} \quad (2)$$

131 where  $k_{ions}$  is the ion collision frequency in the range of  $(1.7 - 2.3) \times 10^{-9} \text{ cm}^3 \text{ s}^{-1}$  (Ehn et al., 2014);  $RT$  is  
132 the residence time in the charger and  $f_{inlet}$  represents the fractions of target species that passed through the  
133 inlet.

134 Herein, we apply the  $C$  determined for sulfuric acid (H<sub>2</sub>SO<sub>4</sub>) of  $3.4 \times 10^9 \text{ molecules cm}^{-3} \text{ ncps}^{-1}$  to  
135 semi-quantify the concentrations of OOMs, which is widely used in previous studies (Ehn et al., 2014;  
136 Yan et al., 2021; Yao et al., 2018). Among the low volatility vapors, it had been demonstrated that nitrate  
137 ions exhibit highest charging efficiency toward H<sub>2</sub>SO<sub>4</sub> (Ehn et al., 2014; Hyttinen et al., 2015, 2018; Riva  
138 et al., 2019b). The estimated concentrations of OOMs thus can be considered as the lower limits with an  
139 uncertainty of  $\pm 50\%$  according to error propagation (Ehn et al., 2014). Positive matrix factorization (PMF)  
140 was also performed for the measured species using Source Finder (SoFi, v6.3) based on Igor and run by

141 the multilinear engine (ME-2) as detailed in SI-S3 and Figure S3-S6 (Canonaco et al., 2013).

## 142 **3. Results and discussion**

### 143 **3.1 Chemical characteristic of OOMs**

144 In total, we have identified 562 OOMs, which concentrated in the nC range of 5 to 10, taking up 84.6%  
145 of total OOMs during the whole campaign (unless otherwise stated, all the reported values hereafter were  
146 corresponding to the average of the whole campaign). Possible precursors of C<sub>5-10</sub> OOMs include isoprene  
147 (C<sub>5</sub>), benzene/alkyl benzenes (C<sub>6-10</sub>), aliphatic VOCs (C<sub>5-10</sub>) and monoterpene (C<sub>10</sub>) according to previous  
148 studies (Bianchi et al., 2019; Nie et al., 2022). C<sub>≤4</sub> OOMs only took up a small fraction of 6.7% among  
149 total OOMs and were likely a result of the decomposition from OOMs with large carbon numbers as  
150 suggested by one of our companion studies (Zhang et al., 2022). The rest 8.7% were C<sub>>10</sub> OOMs which  
151 accounted for a dominating fraction (70%, Figure S7) among the extremely low-volatility organic  
152 compounds (ELVOC, C\* < 3 × 10<sup>-5</sup> μg m<sup>-3</sup>) based on a volatility parameterization proposed by Donahue  
153 and co-workers (Donahue et al., 2011, 2012; Schervish and Donahue, 2020), and potentially poses larger  
154 impacts on SOA formation owing to their lower volatility.

155 We further classified the detected OOMs into four groups based on the number of N atoms they  
156 possessed, including non-nitrogen (0N-) OOMs, 1N-OOMs, 2N-OOMs, and 3N-OOMs. Their average  
157 fractional contributions to total OOM concentrations as well as the carbon number (nC) distributions are  
158 shown in Figure 1. We found 1N-OOMs dominated the total OOM concentration with an average fraction  
159 of 50%, followed by 2N-OOMs (26%), demonstrating the dominance of N-containing OOMs among total  
160 OOMs. The 3N-OOMs only took up a small fraction (4%) of total OOMs and the rest 20% was 0N-OOMs.

161 More interestingly, we found 1N-OOMs prevailed among the OOMs with nC ≤ 10, yet 2N-OOMs  
162 dominated the C<sub>>10</sub> OOMs (41.8-84.2%), suggesting the increased importance of multi-step bimolecular  
163 oxidation in the formation of 2N-OOMs with nC > 10. We also note that the fraction of 2N-OOMs increased  
164 stepwise with the increase of nC (Figure 1b) while 3N-OOMs don't exhibit a similar dependence. The  
165 potential reason is that, with the increase of nC, on the one hand, more active sites are potentially provided  
166 to promote the occurrence of multi-step oxidation, but on the other hand, the potential larger steric effect

167 can hinder multi-step oxidation. From our observation, these two factors lead an overall positive coupling  
168 for 2N-OOMs, but result in a non-monotonic trend for 3N-OOMs. Furthermore, these 2N-OOMs with  
169  $nC > 10$  had an average molecular composition of  $C_{12.5}H_{22.7}O_{2.1}(NO_3)_2$ . Assuming the nitrogen atoms are  
170 only associated with nitrate group ( $-ONO_2$ ), the mean double bond equivalent value (DBE) (Nie et al.,  
171 2022; Xu et al., 2021) was 1.15 on the carbon skeleton, suggesting its origination from aliphatic  
172 compounds, such as alkanes, alkenes, etc. (Gong et al., 2005; Mentel et al., 2015; Wang and Hildebrandt  
173 Ruiz, 2018).

174 We thus further classified the 2N-OOMs to their possible VOC precursors following a recently  
175 developed workflow proposed by Nie and co-workers, which is based on the up-to-date understanding of  
176 VOC oxidation and molecular characters (*i.e.*, number of different elements, DBE) as well as PMF results  
177 (Nie et al., 2022), *i.e.*, aromatics ( $2N-OOM_{Aro}$ ), aliphatics ( $2N-OOM_{Ali}$ ), and monoterpene ( $2N-OOM_{MT}$ ).  
178 Note that we group isoprene 2N-OOMs ( $2N-OOM_{Iso}$ ) into  $2N-OOM_{Ali}$  as well because of the low  
179 concentration of isoprene in cold season. As a result, the average fractions of  $2N-OOM_{Aro}$ ,  $2N-OOM_{Ali}$   
180 and  $2N-OOM_{MT}$  among total 2N-OOMs were 16.0%, 64.2% and 15.3%, respectively (Figure 2),  
181 suggesting significant contribution of aliphatic compounds to 2N-OOMs formation. Taken together, the  
182 increased fraction of 2N-OOMs with the increase of  $nC$  and the dominant fraction of  $2N-OOM_{Ali}$  highlight  
183 the significant contribution of high-molecular-weight aliphatic precursors (*i.e.*, intermediate volatility or  
184 semi-volatile organic compounds, I/SVOCs) to high-molecular-weight 2N-OOM formation, which were  
185 potentially important SOA material. We thus focus our attention on the formation of 2N-OOMs in the  
186 following sections.

### 187 **3.2 2N-OOM formation in PM episodes**

188 To investigate the formation mechanisms and factors that may affect the 2N-OOM formation, one  
189 clean day (4<sup>th</sup>-5<sup>th</sup> November) and one polluted day (7<sup>th</sup>-8<sup>th</sup> November) based on the pollution levels, *i.e.*,  
190  $PM_{2.5}$  concentrations, were selected for further analysis. Since OOM formation is directly mediated by  
191 photochemistry or nighttime chemistry, the clean and polluted cases were thus split into one clean daytime  
192 case ( $CL_{day}$ ), one clean nighttime case ( $CL_{night}$ ), one polluted daytime case ( $PL_{day}$ ) and one polluted

193 nighttime case ( $PL_{\text{night}}$ ). Detailed information on durations, pollution levels, meteorological conditions  
194 and 2N-OOM concentrations during these four cases were summarized in Table 1.

195 During the whole campaign, the concentrations of 2N-OOMs ranged from  $1.1 \times 10^6$  to  $42.0 \times 10^6$   
196 molecule  $\text{cm}^{-3}$  as shown in Figure 2. We found the concentrations of 2N-OOMs in the polluted cases were  
197 1.7-2.7 times higher than those in clean cases. Table 1 further indicates that the absolute abundances of  
198 almost 2N-OOM classes were higher during the polluted cases as compared to clean case no matter in the  
199 daytime or nighttime except for the daytime 2N-OOM<sub>Aro</sub>. Specifically, 2N-OOM<sub>Ali</sub> occupied the largest  
200 fractions, which were even higher in polluted cases (66-66%) than those in clean cases (56-61%, Figure  
201 2). Especially for the 2N-OOM<sub>Ali</sub> with  $nC > 10$ , its concentration in polluted cases increased by a factor of  
202 2.3-4.8 compared to the clean cases (Figure 3). From PMF analysis, we also identified a factor  
203 characterized by a series of 2N-OOM<sub>Ali</sub> (*i.e.*,  $C_nH_{2n-2}O_8N_2$ ,  $n=5-11$ ) as the fingerprint molecules (Table  
204 S1). This factor tracks the  $PM_{2.5}$  concentration well especially during PM episodes (Figure S8), likely due  
205 to the availability of adequate aliphatic precursors during pollution episode. Furthermore, 2N-OOM<sub>Ali</sub>  
206 with  $nC > 10$  presented both higher concentrations and fractions during daytime than nighttime cases  
207 (Figure 3), suggesting that the photochemical formation of 2N-OOM<sub>Ali</sub> prevailed compared to nighttime  
208 formation. To compare  $CL_{\text{night}}$  and  $PL_{\text{night}}$ , it was also found that the pollution case would lead enhanced  
209 importance of nighttime formation pathways of 2N-OOM<sub>Ali</sub> with  $nC > 10$ .

210 We note that the fraction of 2N-OOM<sub>Ali</sub> increased during  $CL_{\text{night}}$  primarily due to the more evident  
211 decrease of 2N-OOM<sub>Aro</sub> (Table 1), whose formation is dominated by photochemistry. On the other hand,  
212 the decrease of 2N-OOM<sub>Aro</sub> concentrations at  $PL_{\text{night}}$  was not as obvious as those on  $CL_{\text{night}}$ . Due to the  
213 significant increase of 2N-OOM<sub>Ali</sub> concentration, the fraction of 2N-OOM<sub>Aro</sub> decreased in pollution cases,  
214 but their absolute concentrations only had few changes in the daytime. 2N-OOM<sub>MT</sub> showed significant  
215 higher concentrations but similar fractions in polluted cases. On the other hand, equivalent or even slightly  
216 higher concentrations during nighttime than those in daytime suggest the comparable importance of  
217 nighttime chemistry in 2N-OOM<sub>MT</sub> formation in contrast to 2N-OOM<sub>Ali</sub> and 2N-OOM<sub>Aro</sub>, which will be  
218 discussed in later sections.

219 To summarize, the absolute concentrations of 2N-OOM were greatly affected by the pollution level  
220 for the most cases. Both the concentrations and fractions of 2N-OOM<sub>Ali</sub> were significantly promoted by  
221 pollution condition, whereas the 2N-OOM<sub>Aro</sub> were predominantly affected by photochemical production,  
222 whose formation was less sensitive to pollution levels compared to 2N-OOM<sub>Ali</sub> in the daytime. In contrast,  
223 the absolute concentrations of 2N-OOM<sub>MT</sub> were also significantly influenced by pollution levels but seem  
224 not solely/almost depend on daytime/nighttime formation pathway. In addition, we note that both daytime  
225 photochemistry and nighttime chemistry had profound effects on 2N-OOMs formation under different  
226 pollution levels, presumably depending on availability of the precursors as well as the oxidants. We thus  
227 focus our attention on the formation of 2N-OOMs during daytime versus nighttime in the following  
228 sections.

### 229 **3.3 Daytime vs. nighttime formation of 2N-OOMs**

230 We thus investigate the effects of photochemistry and nighttime chemistry on the formation of  
231 individual 2N-OOMs. While the former is dominated by OH radical oxidation, the latter involves NO<sub>3</sub>  
232 radical oxidation as well as reactions with ozone or other oxidants, *e.g.*, halogen. Herein, we use solar  
233 radiation as a proxy of photochemical reactivity, and the concentrations of NO<sub>3</sub> radical were estimated  
234 assuming that NO<sub>3</sub>, NO<sub>2</sub> and N<sub>2</sub>O<sub>5</sub> were under fast equilibration in troposphere (Brown and Stutz, 2012).  
235 The correlation coefficients (Spearman type) between individual 2N-OOM molecules and solar radiation  
236 ( $R_{2N-OOMs-solar}$ ) or NO<sub>3</sub> radical ( $R_{2N-OOMs-NO_3}$ ) derived from different precursors during the whole campaign  
237 were shown in Figure 4a. It should be noted that the concentrations of 2N-OOMs and NO<sub>3</sub> radicals were  
238 scaled with the boundary layer height before calculating the correlation coefficients here and below for  
239 correcting the effects of meteorological dilution.

240 Both 2N-OOM<sub>Aro</sub> and 2N-OOM<sub>Ali</sub> showed stronger correlations with solar radiation over NO<sub>3</sub>  
241 radicals, indicating their association with daytime photochemistry since benzene/alkyl benzenes and  
242 aliphatic VOCs rapidly react with OH radicals compared to other oxidants, such as NO<sub>3</sub> radicals. This is  
243 also supported by the observation that both 2N-OOM<sub>Aro</sub> and 2N-OOM<sub>Ali</sub> peaked during noontime (12:00-  
244 14:00) as shown in Figure 4b. Similarly, the PMF analysis also distinguished two daytime factors. The

245 daytime factor-1 peaked at around 12:00-14:00 (Table S1) and highly correlated with solar radiation  
246 ( $R=0.57$ ). The fingerprint-molecules of daytime factor-1 are  $C_nH_{2n-4}O_{10}N_2$  ( $n=8-10$ ) with average DBE  
247 values of 2 on the carbon skeleton, suggesting the dominance of 2N-OOMs likely formed from aromatic  
248 precursors. Since each step of OH oxidation of aromatics followed by  $RO_2+NO_x$  termination would  
249 increase the nH by one, this factor is likely dominated by 2N-OOMs formed from two steps of OH-  
250 initiated oxidation from alkylbenzenes given the carbon numbers ranged from 8 to 10.

251 The key fingerprint molecule of daytime factor-2 is  $C_nH_{2n}O_8N_2$  ( $n=4-5$ ) (accounting for 30.8% in the  
252 factor profile), followed by  $C_nH_{2n-2}O_8N_2$  ( $n=5-6$ ) (accounting for 9.7% in the factor profile), which is  
253 likely a result of the decomposition from 2N-OOM<sub>Ali</sub> with large carbon numbers, according to their DBE  
254 values of 0-1 on the carbon skeleton. This aliphatic factor presented even higher correlation with solar  
255 radiation ( $R=0.65$ ), peaking at around 12:00-14:00. Strong daytime peaks together with the good  
256 correlations with irradiation suggest the dominance of photochemical oxidation in the formation of 2N-  
257 OOM<sub>Ali</sub>. For 2N-OOM<sub>Ali</sub>, although it showed strong daytime peak, weak nighttime peak was still observed.  
258 This indicates that although daytime formation of 2N-OOM<sub>Ali</sub> prevails, their nighttime formation still  
259 existed. For example, we have obtained a nighttime factor from PMF analysis (nighttime factor-2), whose  
260 fingerprint molecules are  $C_5H_8O_9N_2$  and  $C_nH_{2n}O_7N_2$  ( $n=5-8$ ).  $C_5H_8O_9N_2$  was likely originated from  
261 isoprene and  $C_nH_{2n}O_7N_2$  were likely from anthropogenic aliphatic precursors.

262 Nighttime chemistry plays a more important role in the formation of 2N-OOM<sub>MT</sub>. This is further  
263 supported by the slightly stronger correlation between 2N-OOM<sub>MT</sub> and  $NO_3$  radicals than solar radiation.  
264 For some specific 2N-OOM<sub>MT</sub> species, the formation is likely a result of  $NO_3$  radical initiated oxidation.  
265 As shown in Figure 5, we have identified a series of 2N-OOM<sub>MT</sub> molecules with molecular composition  
266 of  $C_{10}H_{16}O_{7,9,11}N_2$ , which showed strong positive correlations with  $NO_3$  radical. The occurrence  
267 of propagation reaction from  $RO_2$  to RO was critical to the formation of odd oxygen as proposed in  
268 previous chamber studies (Boyd et al., 2015; Clafin and Ziemann, 2018). Furthermore, under the  
269 nighttime conditions observed in urban Shanghai (Table 1), it is estimated that monoterpenes primarily  
270 react with  $NO_3$ , and the fate of nighttime  $RO_2$ s is dominated by NO, which is clear different from rural

271 environment where NO levels likely drop to near zero after sunset (Romer et al., 2016) and RO<sub>2</sub>s are likely  
272 terminated by NO<sub>3</sub>-RO<sub>2</sub> cross-reactions (Bates et al., 2022). Therefore, formation of C<sub>10</sub>H<sub>16</sub>O<sub>7,9,11</sub>N<sub>2</sub> likely  
273 started with the reaction of monoterpene with NO<sub>3</sub> radicals forming a NO<sub>3</sub>-C<sub>10</sub>H<sub>16</sub> alkyl radical, followed  
274 by the formation of organic peroxy radical (RO<sub>2</sub>) upon addition of O<sub>2</sub>. The RO<sub>2</sub> is then converted to an  
275 alkoxy radical (RO) upon reaction with NO. The autoxidation process would then start and stepwise  
276 introduce O<sub>2</sub> into the molecule, forming a series of more oxygenated RO<sub>2</sub> radicals, *i.e.*, NO<sub>3</sub>-  
277 C<sub>10</sub>H<sub>16</sub>(O)(OO)<sub>n</sub>. The NO termination reaction of these RO<sub>2</sub> radicals would finally result in ONs with  
278 chemical composition of NO<sub>3</sub>-C<sub>10</sub>H<sub>16</sub>(O)(OO)<sub>n</sub>O(NO)O (n=0, 1, 2).

279 On the other hand, the reaction rate between monoterpenes (*i.e.*, alpha-pinene, beta-pinene and  
280 limonene) and NO<sub>3</sub> are about 60,000-140,000 times faster than that between monoterpenes and O<sub>3</sub> at 293K  
281 (MCMv3.1), but the averaged nighttime concentrations of O<sub>3</sub> (22.8 ppb) was only about 18,000 times  
282 higher than that of NO<sub>3</sub> (1.3 ppt). Therefore, NO<sub>3</sub>-initiated oxidation process posed significant impacts on  
283 2N-OOM<sub>MT</sub> formation during nighttime. The 2N-OOM<sub>MT</sub> resulted from NO<sub>3</sub> oxidation is also resolved as  
284 a nighttime factor (nighttime factor-1) from PMF analysis, which tracked the NO<sub>3</sub> concentrations well  
285 (Figure S9, *R*=0.46) and peaked at around 19:00-23:00. Fingerprint molecule of nighttime factor-1 was  
286 mainly including C<sub>10</sub>H<sub>16</sub>O<sub>9</sub>N<sub>2</sub> and C<sub>10</sub>H<sub>16</sub>O<sub>8</sub>N<sub>2</sub>, which is generated from NO<sub>3</sub>-initiated oxidation followed  
287 by NO termination and this process will not change the nH of the parent monoterpene molecule.

### 288 3.4 Oxygenation level of 2N-OOMs

289 We then calculated the average effective oxygen number ( $nO_{\text{eff}} = nO - 2nN$ ) of 2N-OOMs, which is  
290 used to indicate the oxidation state of carbon by excluding the oxygen atoms bonded with nitrogen atoms.  
291 Note that calculation of  $nO_{\text{eff}}$  assumes that the nitrogen atoms are only associated with nitrate group (-  
292 ONO<sub>2</sub>), which is reasonable after excluding nitrophenol peaks. The average  $nO_{\text{eff}}$  of 2N-OOMs from  
293 different precursors in CL<sub>day</sub>, CL<sub>night</sub>, PL<sub>day</sub> and PL<sub>night</sub> were shown in Figure 6 and summarized in Table  
294 S2. 2N-OOM<sub>Aro</sub> had the highest  $nO_{\text{eff}}$  (4.8-5.6), followed by 2N-OOM<sub>MT</sub> (4.5-4.9) and 2N-OOM<sub>Ali</sub> were  
295 of lowest  $nO_{\text{eff}}$  (3.9-4.0). Difference in the oxygenation level of different types of OOMs can be attributed  
296 to the difference in oxidation mechanisms of the initiation reactions. For example, the OH-initiated

297 oxidation of alkanes, aromatics and monoterpene/alkenes would form a  $C_xH_yO_2$  radical,  $C_xH_yO_5$  radical  
298 and  $C_xH_yO_3$  radical, respectively, incorporating different number of oxygen atoms into the original  
299 precursor molecules at the first step of oxidation (MCMv3.1). On the other hand, during the multiple-step  
300 oxidation in daytime, aromatics could still provide more C=C bonds than other precursors after the initial  
301 step which is plausibly capable to further react with OH,  $O_3$  and others oxidants.

302 Furthermore, we also found that regardless of the pollution level, the  $nO_{eff}$  was considerably higher  
303 in daytime cases than that in nighttime cases particularly for 2N-OOM<sub>Aro</sub> and 2N-OOM<sub>MT</sub>, suggesting a  
304 profound effects of photochemistry on the formation of highly oxygenated 2N-OOMs. This is likely  
305 because of the high  $NO_x$  concentrations during the nighttime (Table 1), which could efficiently suppress  
306 the  $RO_2$  radicals from autoxidation reactions forming overall less oxygenated OOM molecules. The effect  
307 of  $NO_x$  on oxygenation levels would be discussed in a subsequent paragraph. The average  $nO_{eff}$  of 2N-  
308 OOM<sub>Ali</sub> in four sub-periods were similar without significant daytime and nighttime difference, ranging  
309 from 3.9-4.0. This could be partly explained by the fact that reactions with oxidants such as OH and  
310 halogen radicals will similarly result in the addition of oxygen atoms by two for alkanes during the first  
311 step of oxidation. Thus, the oxygenation levels of 2N-OOM<sub>Ali</sub> were supposed to be insensitive to the  
312 oxidants in daytime or nighttime.

313 It is known that NO is also critical in determining the fate of  $RO_2$  radical during the oxidation,  
314 forming RO radicals or organonitrates. Formation of RO radicals and organonitrates will have opposite  
315 effects on the oxidation state of the termination products since the former will significantly increase the  
316 oxygenation state of carbon through initiating propagation reactions before termination. We thus explore  
317 the effects of NO as well as the total  $NO_x$  concentrations on the average oxygenation levels of 2N-OOMs  
318 from different precursors during the whole campaign (Figure 7). Consistent with previous studies in  
319 polluted urban environment (Qiao et al., 2021; Yan et al., 2021), the detected 2N-OOMs were also of low  
320 oxygenation with  $nO_{eff}$  of 3.9-5.4 (25-75% percentile) compared to those measured in forest or in  
321 laboratory studies (Berndt et al., 2016; Ehn et al., 2014; Jokinen et al., 2014; Rissanen et al., 2014; Yan et  
322 al., 2016).  $nO_{eff}$  of 2N-OOM<sub>Aro</sub> and 2N-OOM<sub>MT</sub> increased with the decrease of  $NO/NO_x$  concentrations.

323 This is likely due to the prevailing of NO termination reactions because the maximum autoxidation rate  
324 constant of alkylbenzenes with long-chain substituents (e.g., isopropyl-benzene, ethyl-benzene) and  
325 monoterpene are comparable to the bimolecular reaction rate between RO<sub>2</sub> and NO (Bianchi et al., 2019).  
326 The oxygenation levels of 2N-OOM<sub>Ali</sub> appears to be insensitive to the pollution levels and NO/NO<sub>x</sub>  
327 concentrations, which should be further investigated in future studies.

## 328 **4 Conclusion**

329 We report the unambiguous identification of 2N-OOMs as well as other OOMs using an ultra-high-  
330 resolution orbitrap coupled with a nitrate inlet. We found that OOMs distributed in a wide range of carbon  
331 numbers (nC = 4 - 16), among which the 2N-OOMs occupied a considerable fraction (26%) of the total  
332 observed OOMs. During the whole campaign, the 2N-OOM concentrations ranged from  $1.1 \times 10^6$  to  
333  $42.0 \times 10^6$  molecule cm<sup>-3</sup> and concentrated in the nC range of 5 to 10 with high molecular weight (m/z >  
334 350 Th), suggesting their low volatilities and thus potentially high contribution to local SOA formation.

335 Aliphatic, aromatics, and monoterpenes were plausible precursors of 2N-OOMs with a fraction of  
336 64.2%, 16% and 15.4%, respectively. The absolute concentrations of 2N-OOMs were greatly affected by  
337 the pollution level for the most cases. The 2N-OOM<sub>Ali</sub> was found to be the most abundant 2N-OOMs and  
338 its fraction even increased in the polluted day with enhanced proportion of ones with nC>10, probably  
339 due to the high concentrations of aliphatic precursors accompanied with PM episodes. Significant  
340 contribution of long-chain aliphatic compounds (nC > 10) to 2N-OOM formation is also supported by the  
341 observation that 2N-OOM fraction increased with the increase of nC and they are of low DBE values,  
342 likely through multistep bimolecular oxidation. 2N-OOM<sub>Ali</sub> and 2N-OOM<sub>Aro</sub> mainly peaked in daytime  
343 and showed stronger correlations with solar radiation over NO<sub>3</sub> radicals, indicating their association with  
344 daytime photochemistry since benzene/alkyl benzenes and aliphatic hydrocarbons rapidly react with OH  
345 radicals compared with other oxidants, such as NO<sub>3</sub> radicals. In contrast, 2N-OOM<sub>MT</sub> prevailed both in  
346 daytime and nighttime, some specific 2N-OOM<sub>MT</sub> species showed strong positive correlations with NO<sub>3</sub>  
347 radical and were likely a result of NO<sub>3</sub> radical initiated oxidation, suggesting the comparable importance  
348 of nighttime NO<sub>3</sub> chemistry in 2N-OOM<sub>MT</sub> formation. In terms of oxygenation levels, we found that 2N-

349 OOM<sub>Aro</sub> had highest averaged nO<sub>eff</sub> followed by 2N-OOM<sub>MT</sub>. Daytime photochemistry and low NO<sub>x</sub>  
350 concentrations had profound effects on the formation of more oxygenated 2N-OOMs. 2N-OOM<sub>Ali</sub> had the  
351 lowest nO<sub>eff</sub> and had negligible changes under different pollution levels. These results demonstrate the  
352 preference of 2N-OOM formation and the influencing factors in a Chinese megacity involving various  
353 VOC precursors (biogenic VOCs such as monoterpene and anthropogenic VOCs such as aromatics,  
354 aliphatic hydrocarbons) and various atmospheric oxidants (such as OH radical and NO<sub>3</sub> radicals), and  
355 highlight the influence of PM episode.

### 356 **Code/Data availability**

357 Data presented in this paper are available upon request to the corresponding author.

### 358 **Author contributions**

359 CH designed this study. YL, YM, DDH, SL, SJ, and YG conducted the field campaign. YL analyzed  
360 data with contributions from CH and all the other co-authors. YL wrote the manuscript with contributions  
361 from all the other co-authors.

### 362 **Competing interests**

363 The authors declare that they have no conflict of interest.

### 364 **Acknowledgement**

365 This study was financially supported by the Funded by the National Key R&D Program of China  
366 (2022YFC3700205), and China Postdoctoral Science Foundation (2022T150427).

### 367 **Reference**

- 368 Atkinson, R. and Arey, J.: Atmospheric Degradation of Volatile Organic Compounds, *Chem. Rev.*, 103(3),  
369 4605–4638, doi:10.1021/cr0206420, 2003.
- 370 Bates, K. H., Burke, G. J. P., Cope, J. D. and Nguyen, T. B.: Secondary organic aerosol and organic  
371 nitrogen yields from the nitrate radical (NO<sub>3</sub>) oxidation of alpha-pinene from various RO<sub>2</sub> fates,  
372 *Atmos. Chem. Phys.*, 22(2), 1467–1482, doi:10.5194/acp-22-1467-2022, 2022.
- 373 Berndt, T., Richters, S., Jokinen, T., Hyttinen, N., Kurtén, T., Otkjær, R. V., Kjaergaard, H. G., Stratmann,  
374 F., Herrmann, H., Sipilä, M., Kulmala, M. and Ehn, M.: Hydroxyl radical-induced formation of

375 highly oxidized organic compounds, *Nat. Commun.*, 7(13677), doi:10.1038/ncomms13677, 2016.

376 Berndt, T., Scholz, W., Mentler, B., Fischer, L., Herrmann, H., Kulmala, M. and Hansel, A.: Accretion  
377 Product Formation from Self- and Cross-Reactions of RO<sub>2</sub> Radicals in the Atmosphere, *Angew.*  
378 *Chemie - Int. Ed.*, 57(14), 3820–3824, doi:10.1002/anie.201710989, 2018.

379 Bianchi, F., Kurtén, T., Riva, M., Mohr, C., Rissanen, M. P., Roldin, P., Berndt, T., Crouse, J. D.,  
380 Wennberg, P. O., Mentel, T. F., Wildt, J., Junninen, H., Jokinen, T., Kulmala, M., Worsnop, D. R.,  
381 Thornton, J. A., Donahue, N., Kjaergaard, H. G. and Ehn, M.: Highly Oxygenated Molecules (HOM)  
382 from Gas-Phase Autoxidation Involving Organic Peroxy Radicals: A Key Contributor to  
383 Atmospheric Aerosol, *Chem. Rev.*, 119, 3472–3509, doi:10.1021/acs.chemrev.8b00395, 2019.

384 Boyd, C. M., Sanchez, J., Xu, L., Eugene, A. J., Nah, T., Tuet, W. Y., Guzman, M. I. and Ng, N. L.:  
385 Secondary organic aerosol formation from the  $\beta$ -pinene+NO<sub>3</sub> system: Effect of humidity and peroxy  
386 radical fate, *Atmos. Chem. Phys.*, 15(13), 7497–7522, doi:10.5194/acp-15-7497-2015, 2015.

387 Brown, S. S. and Stutz, J.: Nighttime radical observations and chemistry, *Chem. Soc. Rev.*, 41, 6405–  
388 6447, doi:10.1039/c2cs35181a, 2012.

389 Cai, R., Li, Y., Clément, Y., Li, D., Dubois, C., Fabre, M., Besson, L., Perrier, S., George, C., Ehn, M.,  
390 Huang, C., Yi, P., Ma, Y. and Riva, M.: Orbitool: A software tool for analyzing online Orbitrap mass  
391 spectrometry data, *Atmos. Meas. Tech.*, 14, 2377–2387, doi:10.5194/amt-2020-267, 2020.

392 Canonaco, F., Crippa, M., Slowik, J. G., Baltensperger, U. and Prévôt, A. S. H. H.: SoFi, an IGOR-based  
393 interface for the efficient use of the generalized multilinear engine (ME-2) for the source  
394 apportionment: ME-2 application to aerosol mass spectrometer data, *Atmos. Meas. Tech.*, 6(12),  
395 3649–3661, doi:10.5194/amt-6-3649-2013, 2013.

396 Claflin, M. S. and Ziemann, P. J.: Identification and Quantitation of Aerosol Products of the Reaction of  
397  $\beta$ -Pinene with NO<sub>3</sub> Radicals and Implications for Gas- and Particle-Phase Reaction Mechanisms, *J.*  
398 *Phys. Chem. A*, 122(14), 3640–3652, doi:10.1021/acs.jpca.8b00692, 2018.

399 Ditto, J. C., Joo, T., Slade, J. H., Shepson, P. B., Ng, N. L. and Gentner, D. R.: Nontargeted Tandem Mass  
400 Spectrometry Analysis Reveals Diversity and Variability in Aerosol Functional Groups across

401 Multiple Sites, Seasons, and Times of Day, *Environ. Sci. Technol. Lett.*, 7(2), 60–69,  
402 doi:10.1021/acs.estlett.9b00702, 2020.

403 Donahue, N. M., Robinson, A. L. and Pandis, S. N.: Atmospheric organic particulate matter: From smoke  
404 to secondary organic aerosol, *Atmos. Environ.*, 43(1), 94–106, doi:10.1016/j.atmosenv.2008.09.055,  
405 2009.

406 Donahue, N. M., Epstein, S. A., Pandis, S. N. and Robinson, A. L.: A two-dimensional volatility basis set:  
407 1. organic-aerosol mixing thermodynamics, *Atmos. Chem. Phys.*, 11(7), 3303–3318,  
408 doi:10.5194/acp-11-3303-2011, 2011.

409 Donahue, N. M., Kroll, J. H., Pandis, S. N. and Robinson, A. L.: A two-dimensional volatility basis set-  
410 Part 2: Diagnostics of organic-aerosol evolution, *Atmos. Chem. Phys.*, 12(2), 615–634,  
411 doi:10.5194/acp-12-615-2012, 2012.

412 Ehn, M., Thornton, J. A., Kleist, E., Sipilä, M., Junninen, H., Pullinen, I., Springer, M., Rubach, F.,  
413 Tillmann, R., Lee, B., Lopez-Hilfiker, F., Andres, S., Acir, I.-H. H., Rissanen, M., Jokinen, T.,  
414 Schobesberger, S., Kangasluoma, J., Kontkanen, J., Nieminen, T., Kurtén, T., Nielsen, L. B.,  
415 Jørgensen, S., Kjaergaard, H. G., Canagaratna, M., Maso, M. D., Berndt, T., Petäjä, T., Wahner, A.,  
416 Kerminen, V.-M. M., Kulmala, M., Worsnop, D. R., Wildt, J. and Mentel, T. F.: A large source of  
417 low-volatility secondary organic aerosol, *Nature*, 506(7489), 476–479, doi:10.1038/nature13032,  
418 2014.

419 Garmash, O., Rissanen, M. P., Pullinen, I., Schmitt, S., Kausiala, O., Tillmann, R., Zhao, D., Percival, C.,  
420 Bannan, T. J., Priestley, M., Hallquist, A. M., Kleist, E., Kiendler-Scharr, A., Hallquist, M., Berndt,  
421 T., McFiggans, G., Wildt, J., Mentel, T. F. and Ehn, M.: Multi-generation OH oxidation as a source  
422 for highly oxygenated organic molecules from aromatics, *Atmos. Chem. Phys.*, 20(1), 515–537,  
423 doi:10.5194/acp-20-515-2020, 2020.

424 Gong, H., Matsunaga, A. and Ziemann, P. J.: Products and mechanism of secondary organic aerosol  
425 formation from reactions of linear alkenes with NO<sub>3</sub> Radicals, *J. Phys. Chem. A*, 109(19), 4312–  
426 4324, doi:10.1021/jp058024l, 2005.

427 Hallquist, M., Wenger, J. C., Baltensperger, U., Rudich, Y., Simpson, D., Claeys, M., Dommen, J.,  
428 Donahue, N. M., George, C., Goldstein, A. H., Hamilton, J. F., Herrmann, H., Hoffmann, T., Iinuma,  
429 Y., Jang, M., Jenkin, M. E., Jimenez, J. L., Kiendler-Scharr, A., Maenhaut, W., McFiggans, G.,  
430 Mentel, T. F., Monod, A., Prévôt, A. S. H., Seinfeld, J. H., Surratt, J. D., Szmigielski, R. and Wildt,  
431 J.: The formation, properties and impact of secondary organic aerosol: Current and emerging issues,  
432 *Atmos. Chem. Phys.*, 9(14), 5155–5236, doi:10.5194/acp-9-5155-2009, 2009.

433 Heinritzi, M., Simon, M., Steiner, G., Wagner, A. C., K<sup>??</sup>rten, A., Hansel, A. and Curtius, J.:  
434 Characterization of the mass-dependent transmission efficiency of a CIMS, *Atmos. Meas. Tech.*, 9(4),  
435 1449–1460, doi:10.5194/amt-9-1449-2016, 2016.

436 Hyttinen, N., Kupiainen-Määttä, O., Rissanen, M. P., Muuronen, M., Ehn, M. and Kurtén, T.: Modeling  
437 the Charging of Highly Oxidized Cyclohexene Ozonolysis Products Using Nitrate-Based Chemical  
438 Ionization, *J. Phys. Chem. A*, 119(24), 6339–6345, doi:10.1021/acs.jpca.5b01818, 2015.

439 Hyttinen, N., Otkjær, R. V., Iyer, S., Kjaergaard, H. G., Rissanen, M. P., Wennberg, P. O. and Kurtén, T.:  
440 Computational Comparison of Different Reagent Ions in the Chemical Ionization of Oxidized  
441 Multifunctional Compounds, *J. Phys. Chem. A*, 122(1), 269–279, doi:10.1021/acs.jpca.7b10015,  
442 2018.

443 Jimenez, J. L., Canagaratna, M. R., Donahue, N. M., Prevot, A. S. H. H., Zhang, Q., Kroll, J. H., DeCarlo,  
444 P. F., Allan, J. D., Coe, H., Ng, N. L., Aiken, A. C., Docherty, K. S., Ulbrich, I. M., Grieshop, A. P.,  
445 Robinson, A. L., Duplissy, J., Smith, J. D., Wilson, K. R., Lanz, V. A., Hueglin, C., Sun, Y. L., Tian,  
446 J., Laaksonen, A., Raatikainen, T., Rautiainen, J., Vaattovaara, P., Ehn, M., Kulmala, M., Tomlinson,  
447 J. M., Collins, D. R., Cubison, M. J., Dunlea, J., Huffman, J. A., Onasch, T. B., Alfarra, M. R.,  
448 Williams, P. I., Bower, K., Kondo, Y., Schneider, J., Drewnick, F., Borrmann, S., Weimer, S.,  
449 Demerjian, K., Salcedo, D., Cottrell, L., Griffin, R., Takami, A., Miyoshi, T., Hatakeyama, S.,  
450 Shimono, A., Sun, J. Y., Zhang, Y. M., Dzepina, K., Kimmel, J. R., Sueper, D., Jayne, J. T., Herndon,  
451 S. C., Trimborn, A. M., Williams, L. R., Wood, E. C., Middlebrook, A. M., Kolb, C. E., Baltensperger,  
452 U., Worsnop, D. R., Dunlea, E. J., Huffman, J. A., Onasch, T. B., Alfarra, M. R., Williams, P. I.,

453 Bower, K., Kondo, Y., Schneider, J., Drewnick, F., Borrmann, S., Weimer, S., Demerjian, K.,  
454 Salcedo, D., Cottrell, L., Griffin, R., Takami, A., Miyoshi, T., Hatakeyama, S., Shimono, A., Sun, J.  
455 Y., Zhang, Y. M., Dzepina, K., Kimmel, J. R., Sueper, D., Jayne, J. T., Herndon, S. C., Trimborn, A.  
456 M., Williams, L. R., Wood, E. C., Middlebrook, A. M., Kolb, C. E., Baltensperger, U. and Worsnop,  
457 D. R.: Evolution of Organic Aerosols in the Atmosphere, *Science* (80-. ), 326(5959), 1525–1529,  
458 doi:10.1126/science.1180353, 2009.

459 Jokinen, T., Sipilä, M., Richters, S., Kerminen, V. M., Paasonen, P., Stratmann, F., Worsnop, D., Kulmala,  
460 M., Ehn, M., Herrmann, H. and Berndt, T.: Rapid autoxidation forms highly oxidized RO<sub>2</sub> radicals  
461 in the atmosphere, *Angew. Chemie Int. Ed.*, 53, 14596–14600, doi:10.1002/anie.201408566, 2014.

462 Jokinen, T., Berndt, T., Makkonen, R., Kerminen, V.-M., Junninen, H., Paasonen, P., Stratmann, F.,  
463 Herrmann, H., Guenther, A. B., Worsnop, D. R., Kulmala, M., Ehn, M. and Sipilä, M.: Production  
464 of extremely low volatile organic compounds from biogenic emissions: Measured yields and  
465 atmospheric implications, *Proc. Natl. Acad. Sci.*, 112(23), 7123–7128,  
466 doi:10.1073/pnas.1423977112, 2015.

467 Junninen, H., Ehn, M., Petäjä, Luosujärvi, L., Kotiaho, T., Kostianinen, R., Rohner, U., Gonin, M., Fuhrer,  
468 K., Kulmala, M. and Worsnop, D. R.: A high-resolution mass spectrometer to measure atmospheric  
469 ion composition, *Atmos. Meas. Tech.*, 3(4), 1039–1053, doi:10.5194/amt-3-1039-2010, 2010.

470 Kenagy, H. S., Present, P. S. R., Wooldridge, P. J., Nault, B. A., Campuzano-jost, P., Day, D. A., Jimenez,  
471 J. L., Zare, A., Pye, H. O. T., Yu, J., Song, C. H., Blake, D. R., Woo, J., Kim, Y. and Cohen, R. C.:  
472 Contribution of Organic Nitrates to Organic Aerosol over South Korea during KORUS-AQ, *Environ.*  
473 *Sci. Technol.*, 55, 16326–16338, doi:10.1021/acs.est.1c05521, 2021.

474 Kiendler-Scharr, A., Mensah, A. A., Friese, E., Topping, D., Nemitz, E., Prevot, A. S. H., Äijälä, M.,  
475 Allan, J., Canonaco, F., Canagaratna, M., Carbone, S., Crippa, M., Dall'Osto, M., Day, D. A., De  
476 Carlo, P., Di Marco, C. F., Elbern, H., Eriksson, A., Freney, E., Hao, L., Herrmann, H., Hildebrandt,  
477 L., Hillamo, R., Jimenez, J. L., Laaksonen, A., McFiggans, G., Mohr, C., O'Dowd, C., Otjes, R.,  
478 Ovadnevaite, J., Pandis, S. N., Poulain, L., Schlag, P., Sellegri, K., Swietlicki, E., Tiitta, P.,

479 Vermeulen, A., Wahner, A., Worsnop, D. and Wu, H. C.: Ubiquity of organic nitrates from nighttime  
480 chemistry in the European submicron aerosol, *Geophys. Res. Lett.*, 43(14), 7735–7744,  
481 doi:10.1002/2016GL069239, 2016.

482 Lee, B. H., Mohr, C., Lopez-Hilfiker, F. D., Lutz, A., Hallquist, M., Lee, L., Romer, P., Cohen, R. C.,  
483 Iyer, S., Kurtén, T., Hu, W., Day, D. A., Campuzano-Jost, P., Jimenez, J. L., Xu, L., Ng, N. L., Guo,  
484 H., Weber, R. J., Wild, R. J., Brown, S. S., Koss, A., De Gouw, J., Olson, K., Goldstein, A. H., Seco,  
485 R., Kim, S., McAvey, K., Shepson, P. B., Starn, T., Baumann, K., Edgerton, E. S., Liu, J., Shilling,  
486 J. E., Miller, D. O., Brune, W., Schobesberger, S., D’Ambro, E. L. and Thornton, J. A.: Highly  
487 functionalized organic nitrates in the southeast United States: Contribution to secondary organic  
488 aerosol and reactive nitrogen budgets, *Proc. Natl. Acad. Sci. U. S. A.*, 113(6), 1516–1521,  
489 doi:10.1073/pnas.1508108113, 2016.

490 Lee Ng, N., Brown, S. S., Archibald, A. T., Atlas, E., Cohen, R. C., Crowley, J. N., Day, D. A., Donahue,  
491 N. M., Fry, J. L., Fuchs, H., Griffin, R. J., Guzman, M. I., Herrmann, H., Hodzic, A., Iinuma, Y.,  
492 Kiendler-Scharr, A., Lee, B. H., Luecken, D. J., Mao, J., McLaren, R., Mutzel, A., Osthoff, H. D.,  
493 Ouyang, B., Picquet-Varrault, B., Platt, U., Pye, H. O. T., Rudich, Y., Schwantes, R. H., Shiraiwa,  
494 M., Stutz, J., Thornton, J. A., Tilgner, A., Williams, B. J. and Zaveri, R. A.: Nitrate radicals and  
495 biogenic volatile organic compounds: Oxidation, mechanisms, and organic aerosol, *Atmos. Chem.*  
496 *Phys.*, 17(3), 2103–2162, doi:10.5194/acp-17-2103-2017, 2017.

497 Liebmann, J., Sobanski, N., Schuladen, J., Karu, E., Hellén, H., Hakola, H., Zha, Q., Ehn, M., Riva, M.,  
498 Williams, J., Fischer, H., Lelieveld, J. and Crowley, J. N.: Alkyl nitrates in the boreal forest:  
499 Formation via the NO<sub>3</sub>, OH and O<sub>3</sub> induced oxidation of BVOCs and ambient lifetimes, *Atmos.*  
500 *Chem. Phys. Discuss.*, (3), 1–23, doi:10.5194/acp-2019-463, 2019.

501 Lin, C., Huang, R. J., Duan, J., Zhong, H. and Xu, W.: Primary and Secondary Organic Nitrate in  
502 Northwest China: A Case Study, *Environ. Sci. Technol. Lett.*, 8(11), 947–953,  
503 doi:10.1021/acs.estlett.1c00692, 2021.

504 Mentel, T. F., Springer, M., Ehn, M., Kleist, E., Pullinen, I., Kurtén, T., Rissanen, M., Wahner, A. and

505 Wildt, J.: Formation of highly oxidized multifunctional compounds: autoxidation of peroxy radicals  
506 formed in the ozonolysis of alkenes—deduced from structure–product relationships, *Atmos. Chem.*  
507 *Phys. Discuss.*, 15(2), 2791–2851, doi:10.5194/acpd-15-2791-2015, 2015.

508 Nie, W., Yan, C., Huang, D. D., Wang, Z., Liu, Y., Qiao, X., Guo, Y., Tian, L., Zheng, P., Xu, Z., Li, Y.,  
509 Xu, Z., Qi, X., Sun, P., Wang, J., Zheng, F., Li, X., Yin, R., Dallenbach, K. R., Bianchi, F., Petäjä,  
510 T., Zhang, Y., Wang, M., Schervish, M., Wang, S., Qiao, L., Wang, Q., Zhou, M., Wang, H., Yu, C.,  
511 Yao, D., Guo, H., Ye, P., Lee, S., Li, Y. J., Liu, Y., Chi, X., Kerminen, V.-M., Ehn, M., Donahue, N.  
512 M., Wang, T., Huang, C., Kulmala, M., Worsnop, D., Jiang, J. and Ding, A.: Secondary organic  
513 aerosol formed by condensing anthropogenic vapours over China’s megacities, *Nat. Geosci.*, 15,  
514 255–261, doi:10.1038/s41561-022-00922-5, 2022.

515 Pye, H. O. T., D’Ambro, E. L., Lee, B. H., Schobesberger, S., Takeuchi, M., Zhao, Y., Lopez-Hilfiker, F.,  
516 Liu, J., Shilling, J. E., Xing, J., Mathur, R., Middlebrook, A. M., Liao, J., Welti, A., Graus, M.,  
517 Warneke, C., de Gouw, J. A., Holloway, J. S., Ryerson, T. B., Pollack, I. B. and Thornton, J. A.:  
518 Anthropogenic enhancements to production of highly oxygenated molecules from autoxidation, *Proc.*  
519 *Natl. Acad. Sci. U. S. A.*, 116(14), 6641–6646, doi:10.1073/pnas.1810774116, 2019.

520 Qiao, X., Yan, C., Li, X., Guo, Y., Yin, R., Deng, C., Li, C., Nie, W., Wang, M., Cai, R., Huang, D., Wang,  
521 Z., Yao, L., Worsnop, D. R., Bianchi, F., Liu, Y., Donahue, N. M., Kulmala, M. and Jiang, J.:  
522 Contribution of Atmospheric Oxygenated Organic Compounds to Particle Growth in an Urban  
523 Environment, *Environ. Sci. Technol.*, doi:10.1021/acs.est.1c02095, 2021.

524 Rissanen, M. P., Kurtén, T., Sipilä, M., Thornton, J. A., Kangasluoma, J., Sarnela, N., Junninen, H.,  
525 Jørgensen, S., Schallhart, S., Kajos, M. K., Taipale, R., Springer, M., Mentel, T. F., Ruuskanen, T.,  
526 Petäjä, T., Worsnop, D. R., Kjaergaard, H. G. and Ehn, M.: The formation of highly oxidized  
527 multifunctional products in the ozonolysis of cyclohexene, *J. Am. Chem. Soc.*, 136(44), 15596–  
528 15606, doi:10.1021/ja507146s, 2014.

529 Riva, M.: Multiphase Chemistry of Highly Oxidized Molecules: The Case of Organic Hydroperoxides,  
530 *Chem*, 1(4), 526–528, doi:10.1016/j.chempr.2016.09.015, 2016.

531 Riva, M., Ehn, M., Li, D., Tomaz, S., Bourgain, F., Perrier, S. and George, C.: CI-Orbitrap: An Analytical  
532 Instrument to Study Atmospheric Reactive Organic Species, *Anal. Chem.*, 91, 9419–9423,  
533 doi:10.1021/acs.analchem.9b02093, 2019a.

534 Riva, M., Rantala, P., Krechmer, J. E., Peräkylä, O., Zhang, Y., Heikkinen, L., Garmash, O., Yan, C.,  
535 Kulmala, M., Worsnop, D. and Ehn, M.: Evaluating the performance of five different chemical  
536 ionization techniques for detecting gaseous oxygenated organic species, *Atmos. Meas. Tech.*, 12,  
537 2403–2421, doi:10.5194/amt-2018-407, 2019b.

538 Rollins, A. W., Pusede, S., Wooldridge, P., Min, K. E., Gentner, D. R., Goldstein, A. H., Liu, S., Day, D.  
539 A., Russell, L. M., Rubitschun, C. L., Surratt, J. D. and Cohen, R. C.: Gas/particle partitioning of  
540 total alkyl nitrates observed with TD-LIF in Bakersfield, *J. Geophys. Res. Atmos.*, 118(12), 6651–  
541 6662, doi:10.1002/jgrd.50522, 2013.

542 Romer, P. S., Duffey, K. C., Wooldridge, P. J., Allen, H. M., Ayres, B. R., Brown, S. S., Brune, W. H.,  
543 Crouse, J. D., De Gouw, J., Draper, D. C., Feiner, P. A., Fry, J. L., Goldstein, A. H., Koss, A.,  
544 Misztal, P. K., Nguyen, T. B., Olson, K., Teng, A. P., Wennberg, P. O., Wild, R. J., Zhang, L. and  
545 Cohen, R. C.: The lifetime of nitrogen oxides in an isoprene-dominated forest, *Atmos. Chem. Phys.*,  
546 16(12), 7623–7637, doi:10.5194/acp-16-7623-2016, 2016.

547 Schervish, M. and Donahue, N. M.: Peroxy radical chemistry and the volatility basis set, *Atmos. Chem.*  
548 *Phys.*, 20(2), 1183–1199, doi:10.5194/acp-20-1183-2020, 2020.

549 Wang, D. S. and Hildebrandt Ruiz, L.: Chlorine-initiated oxidation of n-alkanes under high NO<sub>x</sub>  
550 conditions: Insights into secondary organic aerosol composition and volatility using a FIGAERO-  
551 CIMS, *Atmos. Chem. Phys. Discuss.*, (x), 1–26, doi:10.5194/acp-2018-443, 2018.

552 Wang, Y., Mehra, A., Krechmer, J., Yang, G., Hu, X., Lu, Y., Lambe, A., Canagaratna, M., Chen, J.,  
553 Worsnop, D., Coe, H. and Wang, L.: Oxygenated products formed from OH-initiated reactions of  
554 trimethylbenzene: Autoxidation and accretion, *Atmos. Chem. Phys.*, 20, 9563–9579,  
555 doi:10.5194/acp-2020-165, 2020.

556 Xu, L., Suresh, S., Guo, H., Weber, R. J. and Ng, N. L.: Aerosol characterization over the southeastern

557 United States using high-resolution aerosol mass spectrometry: Spatial and seasonal variation of  
558 aerosol composition and sources with a focus on organic nitrates, *Atmos. Chem. Phys.*, 15(13), 7307–  
559 7336, doi:10.5194/acp-15-7307-2015, 2015.

560 Xu, Z. N., Nie, W., Liu, Y. L., Sun, P., Huang, D. D., Yan, C., Krechmer, J., Ye, P. L., Xu, Z., Qi, X. M.,  
561 Zhu, C. J., Li, Y. Y., Wang, T. Y., Wang, L., Huang, X., Tang, R. Z., Guo, S., Xiu, G. L., Fu, Q. Y.,  
562 Worsnop, D., Chi, X. G. and Ding, A. J.: Multifunctional Products of Isoprene Oxidation in Polluted  
563 Atmosphere and Their Contribution to SOA, *Geophys. Res. Lett.*, 48(1), 1–10,  
564 doi:10.1029/2020GL089276, 2021.

565 Yan, C., Nie, W., Äijälä, M., Rissanen, M. P., Canagaratna, M. R., Massoli, P., Junninen, H., Jokinen, T.,  
566 Sarnela, N., Häme, S. A. K., Schobesberger, S., Canonaco, F., Yao, L., Prévôt, A. S. H., Petäjä, T.,  
567 Kulmala, M., Sipilä, M., Worsnop, D. R. and Ehn, M.: Source characterization of highly oxidized  
568 multifunctional compounds in a boreal forest environment using positive matrix factorization, *Atmos.*  
569 *Chem. Phys.*, 16, 12715–12731, doi:10.5194/acp-16-12715-2016, 2016.

570 Yan, C., Yin, R., Lu, Y., Dada, L., Yang, D., Fu, Y., Kontkanen, J., Deng, C., Garmash, O., Ruan, J.,  
571 Baalbaki, R., Schervish, M., Cai, R., Bloss, M., Chan, T., Chen, T., Chen, Q., Chen, X., Chen, Y.,  
572 Chu, B., Dällenbach, K., Foreback, B., He, X., Heikkinen, L., Jokinen, T., Junninen, H.,  
573 Kangasluoma, J., Kokkonen, T., Kurppa, M., Lehtipalo, K., Li, H., Li, H., Li, X., Liu, Y., Ma, Q.,  
574 Paasonen, P., Rantala, P., Pileci, R. E., Rusanen, A., Sarnela, N., Simonen, P., Wang, S., Wang, W.,  
575 Wang, Y., Xue, M., Yang, G., Yao, L., Zhou, Y., Kujansuu, J., Petäjä, T., Nie, W., Ma, Y., Ge, M.,  
576 He, H., Donahue, N. M., Worsnop, D. R., Veli-Matti Kerminen, Wang, L., Liu, Y., Zheng, J.,  
577 Kulmala, M., Jiang, J. and Bianchi, F.: The Synergistic Role of Sulfuric Acid, Bases, and Oxidized  
578 Organics Governing New-Particle Formation in Beijing, *Geophys. Res. Lett.*, 48, 2020GL091944,  
579 doi:10.1029/2020gl091944, 2021.

580 Yao, L., Garmash, O., Bianchi, F., Zheng, J., Yan, C., Kontkanen, J., Junninen, H., Mazon, S. B., Ehn, M.,  
581 Paasonen, P., Sipilä, M., Wang, M., Wang, X., Xiao, S., Chen, H., Lu, Y., Zhang, B., Wang, D., Fu,  
582 Q., Geng, F., Li, L., Wang, H., Qiao, L., Yang, X., Chen, J., Kerminen, V.-M., Petäjä, T., Worsnop,

583 D. R., Kulmala, M. and Wang, L.: Atmospheric new particle formation from sulfuric acid and amines  
584 in a Chinese megacity, *Science* (80-. ), 361, 278–281, doi:10.1126/science.aao4839, 2018.

585 Ye, C., Yuan, B., Lin, Y., Wang, Z., Hu, W., Li, T., Chen, W., Wu, C., Wang, C., Huang, S., Qi, J., Wang,  
586 B., Wang, C., Song, W., Wang, X., Zheng, E., Krechmer, J. E., Ye, P., Zhang, Z., Wang, X., Worsnop,  
587 D. R. and Shao, M.: Chemical characterization of oxygenated organic compounds in the gas phase  
588 and particle phase using iodide CIMS with FIGAERO in urban air, *Atmos. Chem. Phys.*, 21(11),  
589 8455–8478, doi:10.5194/acp-21-8455-2021, 2021.

590 Yu, K., Zhu, Q., Du, K. and Huan, X. F.: Characterization of nighttime formation of particulate organic  
591 nitrates based on high-resolution aerosol mass spectrometry in an urban atmosphere in China, *Atmos.*  
592 *Chem. Phys.*, 19(7), 5235–5249, doi:10.5194/acp-19-5235-2019, 2019.

593 Zhang, Y., Li, D., Ma, Y., Dubois, C., Wang, X., Perrier, S., Chen, H., Wang, H., Jing, S., Lu, Y., Lou,  
594 S., Yan, C., Nie, W., Chen, J., Huang, C., George, C. and Riva, M.: Field Detection of Highly  
595 Oxygenated Organic Molecules in Shanghai by Chemical Ionization–Orbitrap, *Environ. Sci.*  
596 *Technol.*, doi:10.1021/acs.est.1c08346, 2022.

597 Zhao, Y., Thornton, J. A. and Pye, H. O. T.: Quantitative constraints on autoxidation and dimer formation  
598 from direct probing of monoterpene-derived peroxy radical chemistry, *Proc. Natl. Acad. Sci. U. S.*  
599 *A.*, 115(48), 12142–12147, doi:10.1073/pnas.1812147115, 2018.

600

Table 1 Summary of the four cases including the meteorological conditions and concentrations of trace gases and 2N-OOMs

Case	Time	$\overline{PM_{2.5}}$ ( $\mu\text{g m}^{-3}$ )	$\overline{Solar}$ ( $\text{W m}^{-2}$ )	$\bar{T}$ ( $^{\circ}\text{C}$ )	$\overline{RH}$ (%)	$\overline{[O_3]}$ (ppb)	$\overline{[NO]}$ (ppb)	$\overline{[NO_2]}$ (ppb)	$\overline{[NO_3]}$ (ppt)	$\overline{[2N - OOM_{Aro}]}$ ( $\times 10^6 \text{ cm}^{-3}$ )	$\overline{[2N - OOM_{Alt}]}$ ( $\times 10^6 \text{ cm}^{-3}$ )	$\overline{[2N - OOM_{MT}]}$ ( $\times 10^6 \text{ cm}^{-3}$ )	$\overline{[2N - OOM_{Total}]}$ ( $\times 10^6 \text{ cm}^{-3}$ )
CL <sub>day</sub>	Nov. 4 <sup>th</sup> 12:00 - 14:00	7.5	635.6	18.9	35.2	41.9	3.2	8.2	0.1	6.3	11.7	2.3	20.8
CL <sub>night</sub>	Nov. 4 <sup>th</sup> 23:00 - Nov. 5 <sup>th</sup> 01:00	9.5	2.4	13.0	64.1	8.0	2.9	40.5	0.2	1.3	6.0	2.3	9.8
PL <sub>day</sub>	Nov. 7 <sup>th</sup> 12:00 - 14:00	44.0	384.5	23.9	30.5	73.9	2.2	20.6	0.3	6.4	23.8	4.3	36.2
PL <sub>night</sub>	Nov. 7 <sup>th</sup> 23:00 - Nov. 8 <sup>th</sup> 01:00	60.5	2.5	17.8	44.9	27.2	2.1	38.7	6.2	3.1	17.4	5.3	26.5

## Figure Captions

**Figure 1.** (a) Average mass spectrum of the detected OOMs during the whole campaign. The pie chart shows the fractions of OOMs with different number of nitrogen and carbon atoms; (b) The fractions of 0N-OOMs, 1N-OOMs, 2N-OOMs and 3N-OOMs among total OOMs as a function of carbon number (nC).

**Figure 2.** The timeseries of 2N-OOMs originated from different precursors. Four sub-periods were selected to further investigate the fractional distribution of different type of OOM molecules as shown in the pie chart, including a clean daytime case (12:00 to 14:00 on November 4<sup>th</sup>,  $PM_{2.5}=7.5 \mu\text{g m}^{-3}$ ,  $CL_{\text{day}}$ ), a clean nighttime case (23:00 on November 4<sup>th</sup> to 01:00 on November 5<sup>th</sup>,  $PM_{2.5}=9.5 \mu\text{g m}^{-3}$ ,  $CL_{\text{night}}$ ), a daytime case in a PM episode (12:00 to 14:00 on November 7<sup>th</sup>,  $PM_{2.5}=44.0 \mu\text{g m}^{-3}$ ,  $PL_{\text{day}}$ ) and a nighttime case in a PM episode (23:00 on November 7<sup>th</sup> to 01:00 on November 8<sup>th</sup>,  $PM_{2.5}=60.5 \mu\text{g m}^{-3}$ ,  $PL_{\text{night}}$ ). The sizes of pie charts are scaled to the total concentrations of 2N-OOMs.

**Figure 3.** The fractions of  $2N\text{-OOM}_{\text{Ali}}$  with different carbon numbers in the four cases.

**Figure 4.** (a) Statistical distribution of the correlation coefficients (Spearman type) between 2N-OOMs and solar radiation ( $R_{2N\text{-OOMs} - \text{solar}}$ ) in red and the correlation coefficients between 2N-OOMs and  $[\text{NO}_3]$  ( $R_{2N\text{-OOMs} - \text{NO}_3}$ ) in blue for 2N-OOMs from different precursors. The horizontal lines are the median values, boxes denote the 25th- and 75th- percentile values, and whiskers represent the 10th- and 90th- percentile values. (b) The diel patterns of 2N-OOMs from different precursors.

**Figure 5.** Scatter plot of  $R_{2N\text{-OOMs} - \text{NO}_3}$  against  $R_{2N\text{-OOMs} - \text{solar}}$  for specific 2N-OOM species.

**Figure 6.** The  $nO_{\text{eff}}$  of 2N-OOMs derived from different precursors in the four cases, the error bars represent the standard deviations.

**Figure 7.** Effective oxygen number ( $nO_{\text{eff}}$ ) of 2N-OOMs as a function of (a) NO concentration and (b)  $\text{NO}_x$  concentration. The colored squares represent the real measurements. The filled markers indicate the median values in the range as horizontal error bars show, the vertical error bars denote the 25th- and 75th-percentile values.

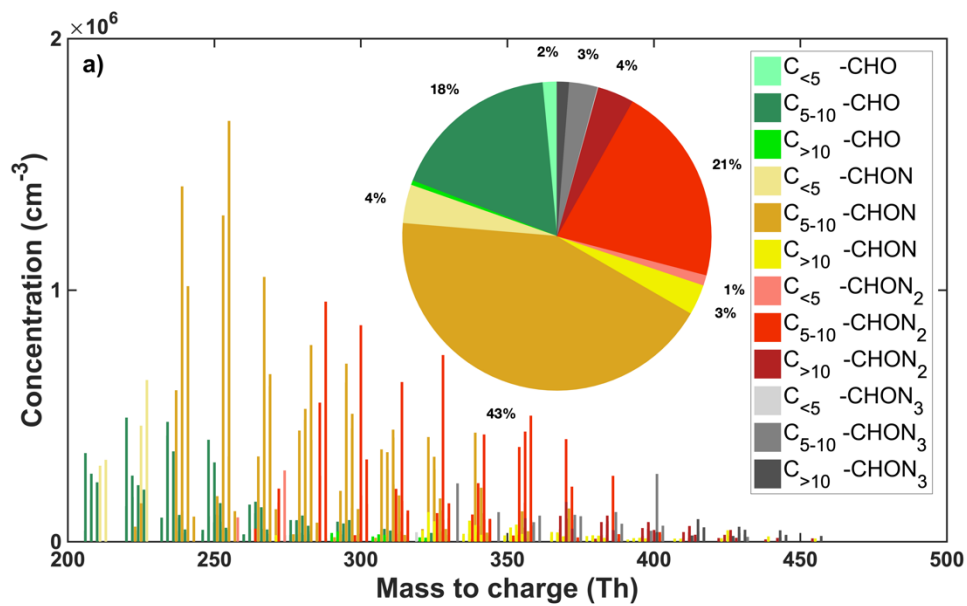


Figure 1a

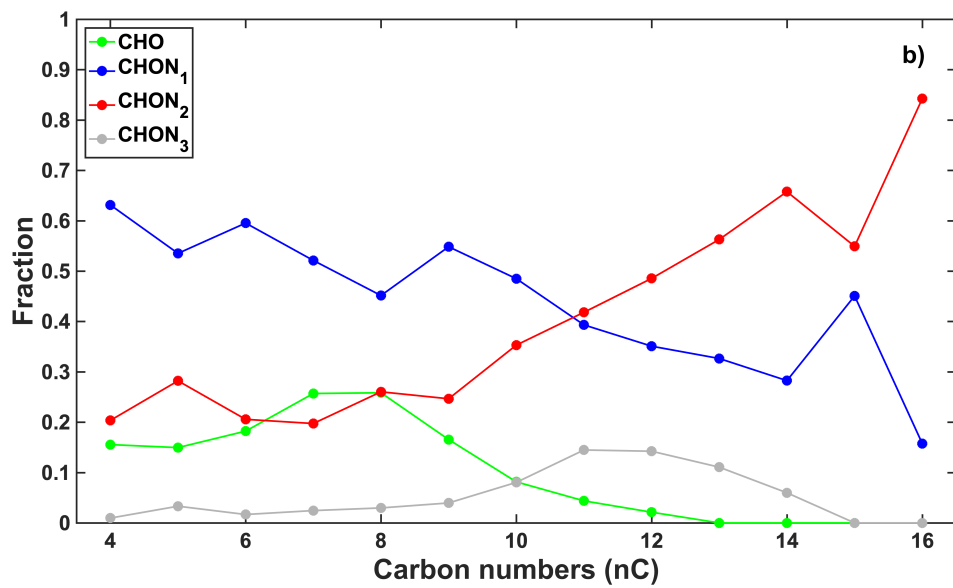


Figure 1b

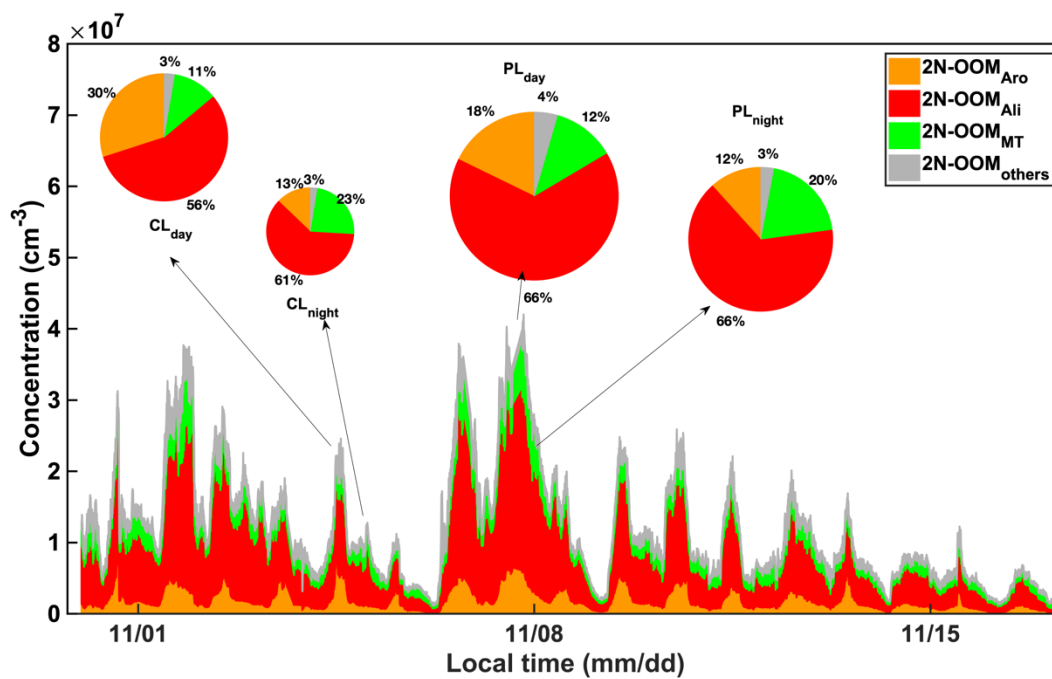


Figure 2

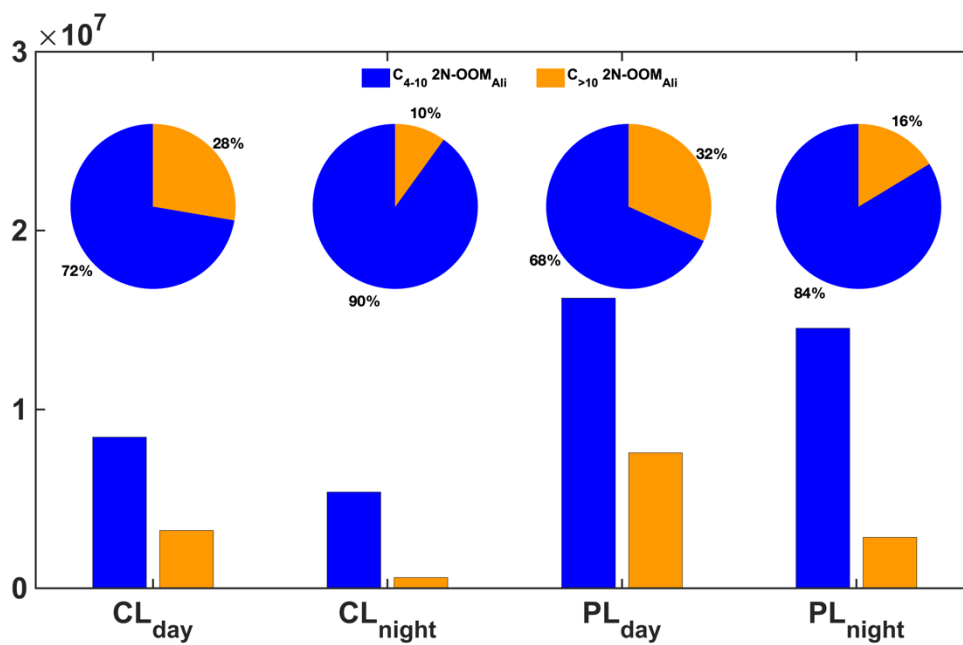


Figure 3

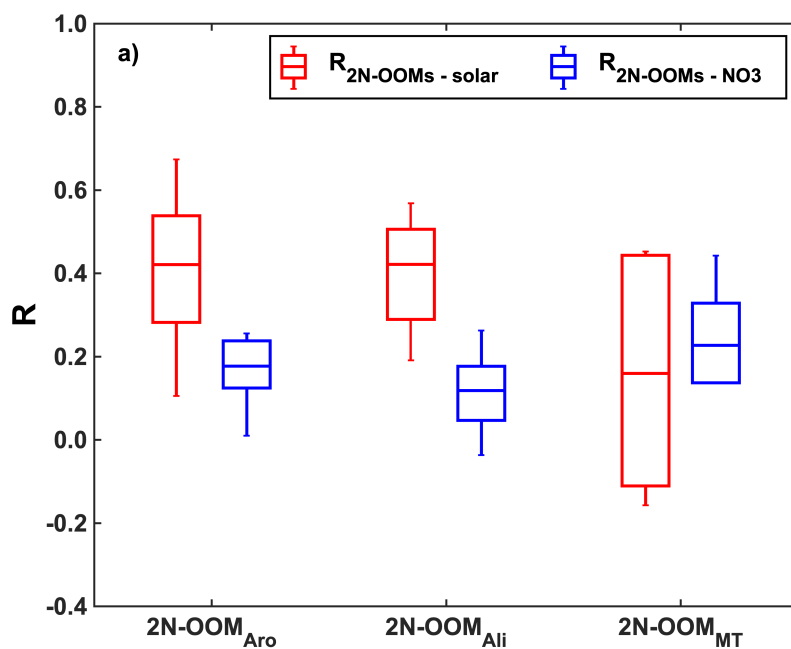


Figure 4a

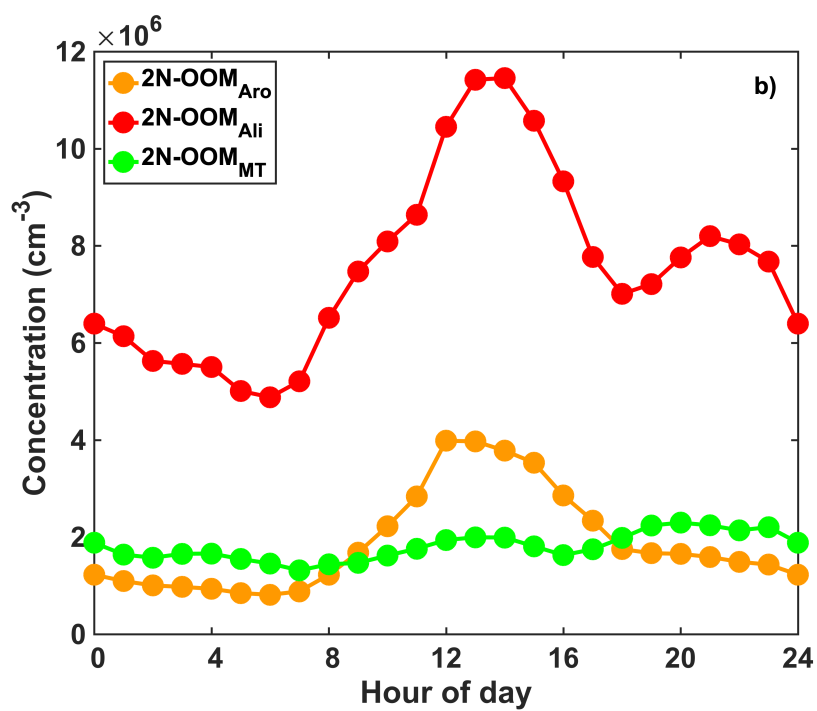


Figure 4b

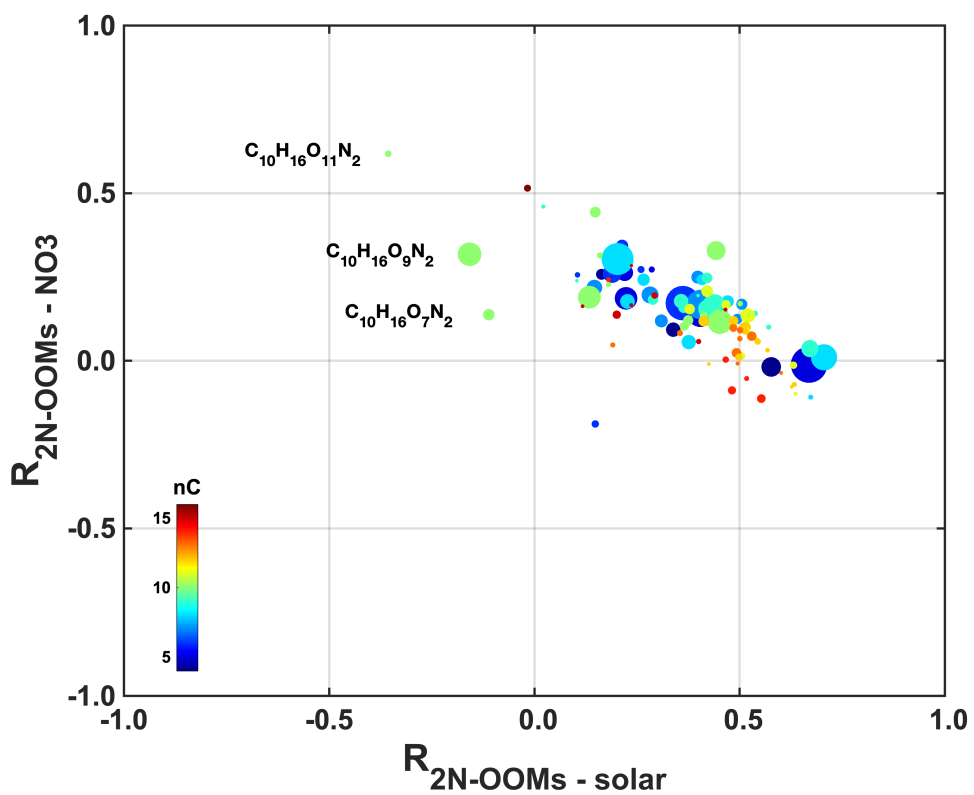


Figure 5

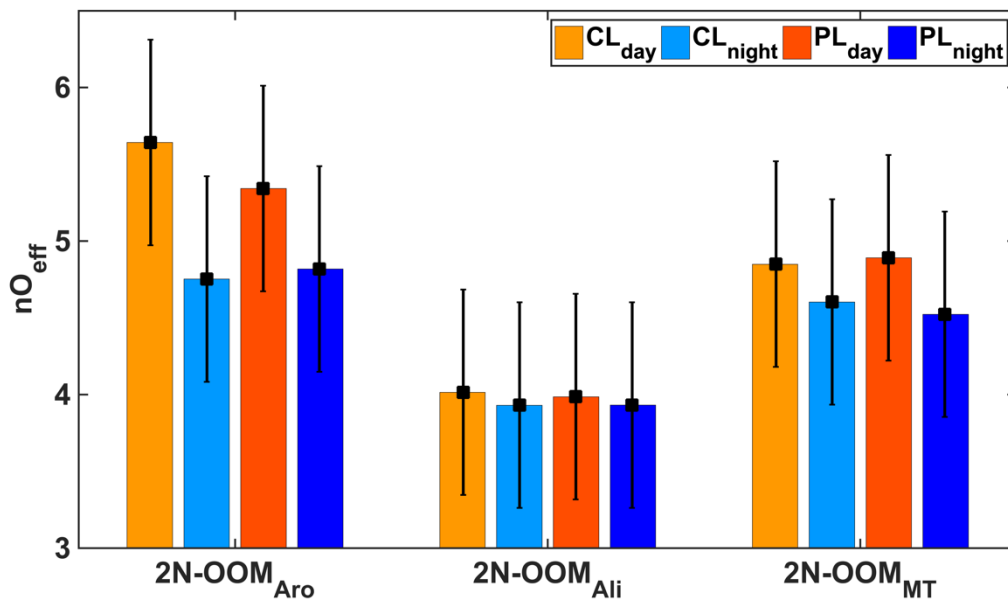


Figure 6

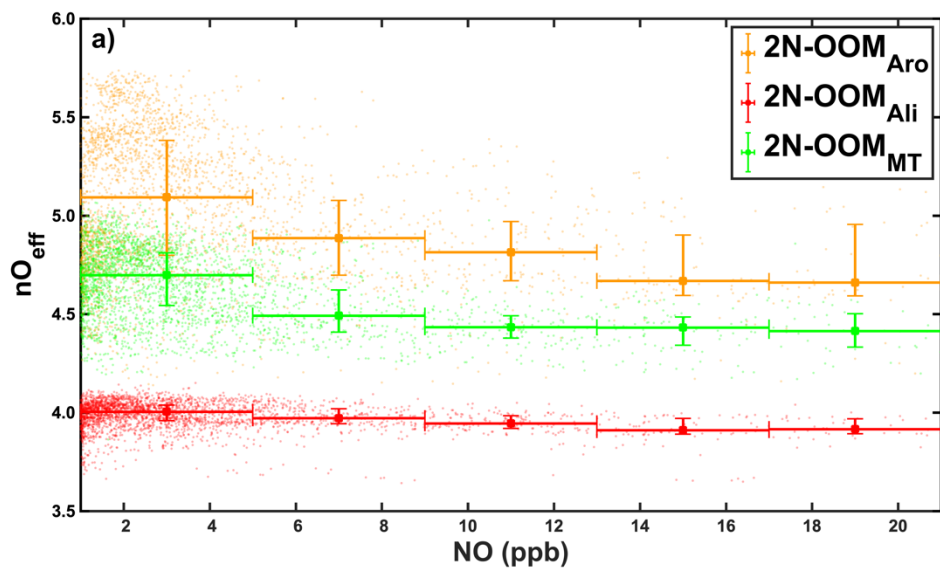


Figure 7a

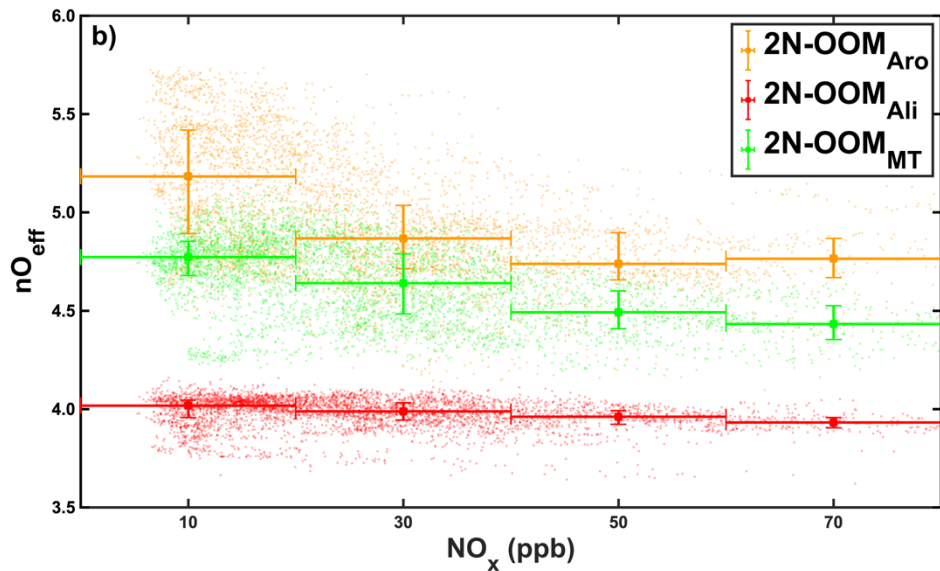


Figure 7b